remote sensing

MDPI

Article

Sharpening the VNIR and SWIR Bands of Sentinel-2A Imagery through Modified Selected and Synthesized Band Schemes

Honglyun Park, Jaewan Choi *, Nyunghee Park and Seokkeun Choi

Department of Civil Engineering, Chungbuk National University, Chungdae-ro 1, Seowon-Gu, Cheongju Chungbuk 28644, Korea; knights111@chungbuk.ac.kr (H.P.); memorial66@chungbuk.ac.kr (N.P.); skchoi@chungbuk.ac.kr (S.C.)

* Correspondence: jaewanchoi@chungbuk.ac.kr; Tel.: +82-43-261-2406

Received: 19 July 2017; Accepted: 16 October 2017; Published: 23 October 2017

Abstract: In this work, the bands of a Sentinel-2A image with spatial resolutions of 20 m and 60 m are sharpened to a spatial resolution of 10 m to obtain visible and near-infrared (VNIR) and shortwave infrared (SWIR) spectral bands with a spatial resolution of 10 m. In particular, we propose a two-step sharpening algorithm for Sentinel-2A imagery based on modified, selected, and synthesized band schemes using layer-stacked bands to sharpen Sentinel-2A images. The modified selected and synthesized band schemes proposed in this study extend the existing band schemes for sharpening Sentinel-2A images with spatial resolutions of 20 m and 60 m to improve the pan-sharpening accuracy by changing the combinations of bands used for multiple linear regression analysis through band-layer stacking. The proposed algorithms are applied to the pan-sharpening algorithm based on component substitution (CS) and a multiresolution analysis (MRA), and our results are then compared to the sharpening results when using sharpening algorithms based on existing band schemes. The experimental results show that the sharpening results from the proposed algorithm are improved in terms of the spatial and spectral properties when compared to existing methods. However, the results of the sharpening algorithm when applied to our modified band schemes show differing tendencies. With the modified, selected band scheme, the sharpening result when applying the CS-based algorithm is higher than the result when applying the MRA-based algorithm. However, the quality of the sharpening results when using the MRA-based algorithm with the modified synthesized band scheme is higher than that when using the CS-based algorithm.

Keywords: Sentinel-2A sharpening; multiple linear regression; component substitution (CS); multiresolution analysis (MRA); band selection and synthesis

1. Introduction

Sentinel-2A satellite images, which support Copernicus land-monitoring research, have various spatial and spectral resolutions and are efficient for acquiring geo-information from the entire Earth [1]. The imagery produced by the Sentinel-2A satellite has spatial resolutions of 10, 20, and 60 m and consists of the visible and near-infrared (VNIR) and shortwave infrared (SWIR) bands. The key mission objectives for Sentinel-2A are to (1) provide systematic global acquisitions of multispectral imagery with a high revisit frequency and high spatial resolution; (2) enhance the continuity of multispectral imagery from the Satellite Pour l'Observation de la Terre (SPOT) series of satellites; and (3) provide observations to produce the next generation of operational products, such as maps of land cover, land-cover changes, and geophysical variables [1]. Recently, studies using the various features of Sentinel-2A imagery have been conducted. Richter et al. [2] used the spectral information of Sentinel-2A for leaf area index (LAI) mapping to create an optimal combination of multispectral

bands. Clevers et al. [3] estimated chlorophyll and nitrogen contents using the red-edge bands on Sentinel-2A and Sentinel-3. Dotzler et al. [4] used Sentinel-2A data to detect drought-stress phenomena in deciduous forests. Most of the aforementioned studies that employed Sentinel-2A data were based on multispectral bands with a spatial resolution of 10 m. When Sentinel-2A imagery bands with spatial resolutions of 20 m and 60 m are used, the integration of Sentinel-2A imagery is difficult because these bands differ in terms of their spatial resolutions. Therefore, Sentinel-2A multispectral imagery, which includes three different spatial resolutions, should be sharpened for various applications, such as image classification, cloud detection, environmental monitoring, change detection, and extraction of geophysical variables. Generally, image fusion, which is also called pan-sharpening, is used to integrate the spatial details of a high-resolution panchromatic image and the color information from a low-resolution multispectral image to produce a high-resolution multispectral image [5]. In remote sensing, the pan-sharpening technique is performed by extracting the spatial details of the panchromatic image and injecting this image into the multispectral image with a low spatial resolution. A variety of pan-sharpening techniques exist that exploit the complementary characteristics of the spatial and spectral resolutions of data [6]. These pan-sharpening techniques are classified into component substitution (CS)-based methods, which effectively reflect spatial characteristics, and multiresolution analysis (MRA)-based methods, which effectively reflect spectral characteristics. The CS-based approach transforms the original multispectral image into a new domain and substitutes one of the components with the high spatial resolution, such as the panchromatic image in the pan-sharpening process [7]. The representative CS-based pan-sharpening methods are intensity-hue saturation (IHS), Brovey transform (BT), and principal component analysis (PCA) fusion [8–10]. However, general CS-based pan-sharpening methods often cause spectral distortion, so many studies have been conducted to overcome these problems. Shah et al. [11] proposed a new pan-sharpening method based on the integration of adaptive PCA and the contourlet transform. Choi et al. [12] proposed a new adaptive CS-based fusion algorithm to minimize spectral distortion, and Kang et al. [13] used the matting model for CS-based pan-sharpening. Meanwhile, the MRA-based approach uses the injection of spatial details from the multiresolution decomposition of a panchromatic image into the resampled multispectral bands [14]. Among the MRA-based methods, the discrete wavelet transform (DWT) and à trous wavelet transform (ATWT) image fusion are used to extract spatial details from panchromatic images [15,16]. Generally, compared to CS-based methods, a DWT and ATWT fusion maintains more spectral characteristics of multispectral images [17]. The ATWT fusion method allows an image to be decomposed into nearly disjoint bandpass channels in the spatial frequency domain, which makes this approach particularly suitable for the fusion of satellite imagery [18]. However, an ATWT fusion cannot effectively capture the geometric structures of images and is prone to generating images with blocking or blurring effects because of aliasing [19]. Garzelli et al. [20] proposed an ATWT-based method with a context-based decision (CBD) injection model. Aiazzi et al. [21] proposed the generalized Laplacian pyramid and context-based decision (GLP-CBD) method.

However, the above algorithms cannot be used when a panchromatic image is not provided along with a multispectral image such as Sentinel-2A. To sharpen a Sentinel-2A image, a specific multispectral band should be defined as an optimal panchromatic band with a 10 m spatial resolution. For example, Vaiopoulos and Karantzalos [22] produced a virtual image that was similar to a panchromatic image using the average of the combined multispectral bands with a 10 m spatial resolution. In addition, Wang et al. [7] fused Sentinel-2A images based on the selected and synthesized band schemes, which were proposed by Selva et al. [23]. Du et al. [24] used the near-infrared (NIR) band with a 10 m spatial resolution as a panchromatic image to sharpen the SWIR band with a 20 m spatial resolution. However, most research has not applied these techniques to sharpen bands with a 60 m spatial resolution, although bands 1, 9, and 10 in Sentinel-2A, which have 60 m spatial resolution, are provided for use in aerosol, water-vapor, biophysical-parameter-extraction, cloud-detection, environmental monitoring, and cirrus-detection correction [25–27].

The main objectives of this work are to develop a new framework to (1) sharpen Sentinel-2A imagery with various spatial resolutions of 20 and 60 m to 10 m using the higher spatial resolution bands at 10 m and (2) enhance the spectral and spatial quality of sharpened Sentinel-2A imagery, compared to existing sharpening algorithm for Sentinel-2A imagery. To sharpen bands with spatial resolutions of 20 and 60 m to high spatial resolution bands (10 m), we propose an extended sharpening framework with two steps based on the modified selected band and synthesized band scheme. The proposed algorithm adds a layer-stacking method in each band scheme and integrates the 20 and 60 m bands using a modulation transfer function (MTF) filter to produce a set of optimal panchromatic images that is most spectrally similar to the multispectral bands with 20 and 60 m spatial resolution. Then, several CS- and MRA-based algorithms, such as the Gram-Schmidt adaptive (GSA), Gram-Schmidt 2 (GS2), generalized intensity-hue-saturation (GIHS) and modulation transfer function-generalized Laplacian pyramid (MTF-GLP) algorithms, are used to sharpen the Sentinel-2A satellite imagery [21,28–30]. We compare the sharpening results of the proposed method with those of the existing selected band and synthesized band schemes to verify the sharpening performance of the proposed method. A comparison between the proposed and existing selected and synthesized methods is conducted through qualitative and quantitative evaluation. Visual inspection is used for qualitative evaluation, and quantitative evaluation is performed by calculating indices to confirm the spectral and spatial accuracy.

This manuscript is organized as follows. Section 2 presents the dataset of Sentinel-2A satellite imagery, the theory of the general pan-sharpening framework, and the drawback of the existing selected and synthesized band scheme. In Section 3, we describe the sharpening methodologies that are based on modified band schemes for Sentinel-2A imagery. The experimental results and discussion are provided in Sections 4 and 5, respectively. Section 6 concludes the manuscript.

2. Previous Studies on Pan-Sharpening of Sentinel-2A

2.1. General Pan-Sharpening Schemes

Pan-sharpening is a technique that produces multispectral images with high spatial resolutions by injecting the spatial information extracted from panchromatic images with high spatial resolution into multispectral images with low spatial resolutions [9,31]. The general pan-sharpening algorithm is defined in Equation (1) [32]:

$$\widehat{\mathbf{MS}}_n = \widetilde{\mathbf{MS}}_n + g_n(\mathbf{P} - \mathbf{I}_L),\ n = 1, \ldots, N \quad (1)$$

where $\widehat{\mathbf{MS}}_n$ is the pan-sharpened multispectral image of the nth band, $\widetilde{\mathbf{MS}}_n$ is the interpolated image of the multispectral image on the scale of $\mathbf{P}$, g_n is the vector of injection gains, $\mathbf{P}$ is the panchromatic image with a high spatial resolution, $\mathbf{I}_L$ is the synthetic intensity image with a low spatial resolution, and N is the number of spectral bands.

As mentioned in Section 1, pan-sharpening algorithms can be classified into CS- and MRA-based techniques, which correspond to the generation method of $\mathbf{I}_L$. In CS-based pan-sharpening algorithms, $\mathbf{I}_L$ is generated using the weighted combinations of a multispectral image with a low spatial resolution. The representative method for creating $\mathbf{I}_L$ is to use the average of multispectral bands or multiple linear regressions between panchromatic and multispectral images. Meanwhile, in MRA-based pan-sharpening algorithms, $\mathbf{I}_L$ is extracted from the panchromatic image as the panchromatic image is decomposed into a lower spatial resolution through wavelet decomposition, image pyramid, and low pass filtering [15]. The pan-sharpened results from CS-based techniques effectively reflect the spatial characteristics of the panchromatic image, although the spectral characteristics of the multispectral image are distorted. Although the pan-sharpened results of MRA-based techniques effectively reflect the spectral characteristics of the multispectral image, these results generate more spatial distortions than CS-based techniques.

In addition to $\mathbf{I}_L$, g_n is one of the most important parameters in both CS- and MRA-based pan-sharpening algorithms. g_n affects the spatial and spectral quality of the pan-sharpened image and functions as a tradeoff parameter between the spectral and spatial distortions [33]. The traditional method for generating g_n is an empirical formula or statistical methods. While CS- and MRA-based algorithms can be classified according to the method for generating $\mathbf{I}_L$, the injection gains reflect the characteristics of specific pan-sharpening algorithms.

2.2. Sentinel-2A Satellite Imagery

The Sentinel-2A images used in this manuscript are level-1C products, which are radiometrically and geometrically corrected datasets. Sentinel-2A satellite imagery consists of ten VNIR bands and three SWIR bands. According to the Sentinel-2A data quality report, the 10th of the thirteen bands in a Sentinel-2A image is an uncalibrated band [34]. This band displays a noise pattern in bright images that are generated by detector saturation. The datasets that are used in this manuscript also contain noise; therefore, twelve bands are used in the experiments, and the 10th band is neglected. Table 1 shows the specifications of the Sentinel-2A images.

Table 1. Specification of the Sentinel-2A satellite imagery.

Band Number		Spatial Resolution (m)	Central Wavelength (nm)	Bandwidth (nm)
VNIR	$\mathbf{MS}_1$	60	443	20
	$\mathbf{MS}_2$	10	490	65
	$\mathbf{MS}_3$	10	560	35
	$\mathbf{MS}_4$	10	665	30
	$\mathbf{MS}_5$	20	705	15
	$\mathbf{MS}_6$	20	740	15
	$\mathbf{MS}_7$	20	783	20
	$\mathbf{MS}_8$	10	842	115
	$\mathbf{MS}_{8a}$	20	865	20
	$\mathbf{MS}_9$	60	945	20
SWIR	$\mathbf{MS}_{10}$	60	1375	30
	$\mathbf{MS}_{11}$	20	1610	90
	$\mathbf{MS}_{12}$	20	2190	180

In this manuscript, we define each band of the Sentinel-2A satellite imagery as follows:

1. $\mathbf{MS10} = \{\mathbf{MS}_2, \mathbf{MS}_3, \mathbf{MS}_4, \mathbf{MS}_8\}$ represents the original multispectral image with a spatial resolution of 10 m, and $\mathbf{MS10}_n$ is the nth band of **MS10** ($n = 1, 2, 3, 4$).
2. $\mathbf{MS20} = \{\mathbf{MS}_5, \mathbf{MS}_6, \mathbf{MS}_7, \mathbf{MS}_{8a}, \mathbf{MS}_{11}, \mathbf{MS}_{12}\}$ represents the original multispectral image with a spatial resolution of 20 m, and $\mathbf{MS20}_m$ is the mth band of **MS20** ($m = 1, 2, \ldots, 6$).
3. $\mathbf{MS60} = \{\mathbf{MS_1}, \mathbf{MS_9}\}$ represents the original multispectral image with a spatial resolution of 60 m, and $\mathbf{MS60}_k$ is the kth band of **MS60** ($k = 1, 2$).

2.3. Existing Algorithm for Pan-Sharpening Sentinel-2A Imagery

Sentinel-2A imagery provides multispectral bands with various spatial resolutions of 10, 20, and 60 m, so traditional pan-sharpening frameworks, such as Equation (1), cannot be directly applied to Sentinel-2A images. As mentioned in Section 1, a panchromatic image of a single band should be defined for sharpening, while Sentinel-2A imagery includes four high spatial resolution bands (**MS10**). Therefore, some researchers proposed algorithms for pan-sharpening Sentinel-2A imagery. The major concept of existing methods for sharpening Sentinel-2A imagery is how to determine the optimal panchromatic images using **MS10**. In the case of Vaiopoulos and Karantzalos [22], $\mathbf{MS}_8$ was directly used as the panchromatic image for sharpening $\mathbf{MS}_{8a}$, while $\mathbf{MS}_5$, $\mathbf{MS}_6$, and $\mathbf{MS}_7$ were sharpened using the average of $\mathbf{MS}_5$ and $\mathbf{MS}_8$ based on the assumption that these bands were spectrally

appropriate for each multispectral band in **MS20**. Wang et al. [7] proposed two schemes that were based on utilizing a hyper-sharpening algorithm, which was developed by Selva et al. [23], to determine the panchromatic image among four bands of **MS10** for the Sentinel-2A-imagery sharpening of **MS20**. These two schemes are known as the selected and synthesized band schemes, which determine the panchromatic image among multispectral images. The objective of these two schemes is to produce optimal panchromatic images using the statistics of multispectral images (e.g., between **MS10** and **MS20**). Existing algorithms are used to sharpen **MS20** using **MS10**, so the two schemes by Wang et al. [7] describe the process of sharpening **MS20**. Based on Equation (1), the sharpening of **MS20** can be applied using Equation (2):

$$\widehat{\mathbf{MS20}}_m = \widetilde{\mathbf{MS20}}_m + g_m(\mathbf{P}_m - \mathbf{I}_m),\ m = 1, \ldots, 6 \tag{2}$$

where $\mathbf{P}_m$ is the optimal panchromatic image according to $\widetilde{\mathbf{MS20}}_m$, and $\mathbf{I}_m$ is the synthetic intensity image from $\mathbf{P}_m$. Therefore, the three parameters g_m, $\mathbf{P}_m$, and $\mathbf{I}_m$ in Equation (2) should be determined for sharpening. $\mathbf{I}_m$ and g_m are determined using the general pan-sharpening algorithm, as mentioned above. The selected and synthesized band scheme is applied to obtain the optimal $\mathbf{P}_m$ for sharpening $\widetilde{\mathbf{MS20}}_m$. $\mathbf{P}_m$ can be determined by defining the function f according to **MS10** and **MS20**, as shown in Equation (3).

$$\mathbf{P}_m = f(\mathbf{MS10},\ \mathbf{MS20}) \tag{3}$$

Spectral distortion occurs in sharpened images if a panchromatic image for extracting the spatial details during pan-sharpening is not covered by the wavelength of each multispectral band or does not have similar spectral characteristics to each multispectral band [12]. Therefore, the function f in Equation (3) is used to generate the optimal $\mathbf{P}_m$, which has the most similar spectral information to **MS20** when using **MS10**. The details of the two schemes are as follows.

2.3.1. Selected Band Scheme

The selected band scheme determines a single band from the set of **MS10** based on which band displays the greatest correlation with each **MS20** band. First, $\mathbf{MS10}_n^L$, which is the downscaled version of $\mathbf{MS10}_n$, is generated using the MTF filter and image degradation and has an identical resolution to **MS20**. Then, the set of the optimal panchromatic band $\mathbf{P}_m$ is selected according to each band of **MS20** by calculating the correlation coefficient between $\mathbf{MS10}_n^L$ and **MS20**. In the selected band scheme, $\mathbf{P}_m$ is directly determined using the band $\mathbf{MS10}_n$ with the maximum correlation with $\mathbf{MS20}_m$. The formulations for determining $\mathbf{P}_m^{sel}$, which is the set of optimal panchromatic bands from the selected band scheme, are shown in Equations (4) and (5):

$$\overline{n} = \text{argmax}_n corr\left(\mathbf{MS10}_n^L,\ \mathbf{MS20}_m\right),\ n = 1, \ldots, 4,\ m = 1, \ldots, 6 \tag{4}$$

$$\mathbf{P}_m^{sel} = \sum_{n=1}^{4} \alpha_{m_n} \mathbf{MS10}_n,\ \text{where } \alpha_{m_n} = \begin{cases} 1,\ if\ \ n = \overline{n} \\ 0,\ otherwise. \end{cases} \tag{5}$$

Through Equations (4) and (5), $\mathbf{P}_m^{sel}$ is iteratively selected for every $\mathbf{MS20}_m$. After determining $\mathbf{P}_m^{sel}$, the synthetic intensity image is calculated to extract the spatial details to be injected. If an MRA-based sharpening algorithm is applied, the synthetic intensity image $\mathbf{I}_m$ is calculated through $\mathbf{P}_m^{sel,L}$, which is a downscaled and resized image of $\mathbf{P}_m^{sel}$, using the MTF filter. For CS-based algorithms, weighted combinations such as the average of $\mathbf{MS20}_m$ or multiple linear regression between $\mathbf{MS20}_m$ and $\mathbf{P}_m^{sel}$ are used to calculate $\mathbf{I}_m$. Based on $\mathbf{P}_m^{sel}$ and $\mathbf{I}_m$, the sharpening of **MS20** can be accomplished using Equation (2). In Equation (2), g_m is extracted using various methods to extract injection gains according to MRA- and CS-based pan-sharpening algorithms.

2.3.2. Synthesized Band Scheme

The synthesized band scheme generates the set of optimal panchromatic images $\mathbf{P}_m$ through the weighted combination of $\mathbf{MS10}_n$. In the synthesized band scheme, $\mathbf{P}_m$ is a completely new band that is spectrally similar to $\mathbf{MS20}_m$ but is not included among the **MS10** bands. First, the $\mathbf{MS10}_n^L$ and $\mathbf{MS20}_m$ images are subjected to multiple regression analysis to generate the set of optimal panchromatic bands $\mathbf{P}_m^{syn}$. This multiple regression analysis can be defined via Equation (6) [14]:

$$\mathbf{MS20}_m = \omega_{m_0} + \sum_{n=1}^{4} \omega_{m_n} \mathbf{MS10}_n^L \tag{6}$$

ω_{m_n}, which are the weight values that correspond to the nth band of $\mathbf{MS10}^L$, are determined using the least-squares method. Then, $\mathbf{P}_m^{syn}$ is calculated using Equation (7):

$$\mathbf{P}_m^{syn} = \omega_{m_0} + \sum_{n=1}^{4} \omega_{m_n} \mathbf{MS10}_n \tag{7}$$

After generating $\mathbf{P}_m^{syn}$, the process is similar to the selected band scheme. The synthesized band scheme is proposed because the $\mathbf{P}_m^{sel}$ values from the selected band scheme may not spectrally match each $\mathbf{MS20}_m$ band, which can create spectral distortion in sharpened images.

2.3.3. Drawbacks of the Existing Band Schemes

The selected and synthesized band scheme can be applied to sharpen **MS60** with **MS10**. However, Sentinel-2A images are individually sharpened for **MS20** and **MS60**, which cannot be applied with the spectral and spatial characteristics according to the overall bands of Sentinel-2A. In addition, some spectral distortion may occur in fused **MS20** and **MS60** images if no bands of **MS10** have similar spectral characteristics to **MS20** and **MS60**. Therefore, the quality of the sharpening is expected to be improved if **MS10**, **MS20**, and **MS60** are simultaneously integrated and used. However, no research on this issue currently exists. In addition, using all the bands in Sentinel-2A imagery minimizes the spectral distortion that forms from the existing technique when performing conventional CS- and MRA- based pan-sharpening.

3. Method

In this work, we extended the sharpening framework based on the selected and synthesized band schemes. In particular, we attempted to increase the spectral and spatial quality of sharpened Sentinel-2A imagery using band-stacked multispectral images. In addition, we sharpened **MS60** utilizing the framework for sharpening **MS20** to generate the optimal $\mathbf{P}_m$ and $\mathbf{I}_m$.

3.1. Study Area and Materials

Two study areas that were covered by 1800 × 1800 pixels in bands with 10 m spatial resolution were selected in this manuscript. These images were taken on 6 August 2016 and 16 October 2016. These two study areas were selected to investigate the effects of different land-cover types on the sharpening process, as shown in Figure 1. Site 1 contains paddy fields, forests, and oceans; Site 2 contains more complex land cover compared to site 1 and includes urban areas, forests, paddies, and bare soil.

3.2. Proposed Band Scheme

The objective of the proposed band scheme is to select the set of optimal panchromatic image **P** and produce the optimal **I** in Equation (1). The proposed selected and synthesized band scheme involves two steps. In the first step, **MS20** is stacked with **MS60**, and then **MS60** is sharpened. In the

second step, sharpened **MS60** are stacked with **MS10** and **MS20**, respectively, and then, **MS20** is sharpened. Figure 2 presents the workflow of the proposed selected and synthesized band scheme.

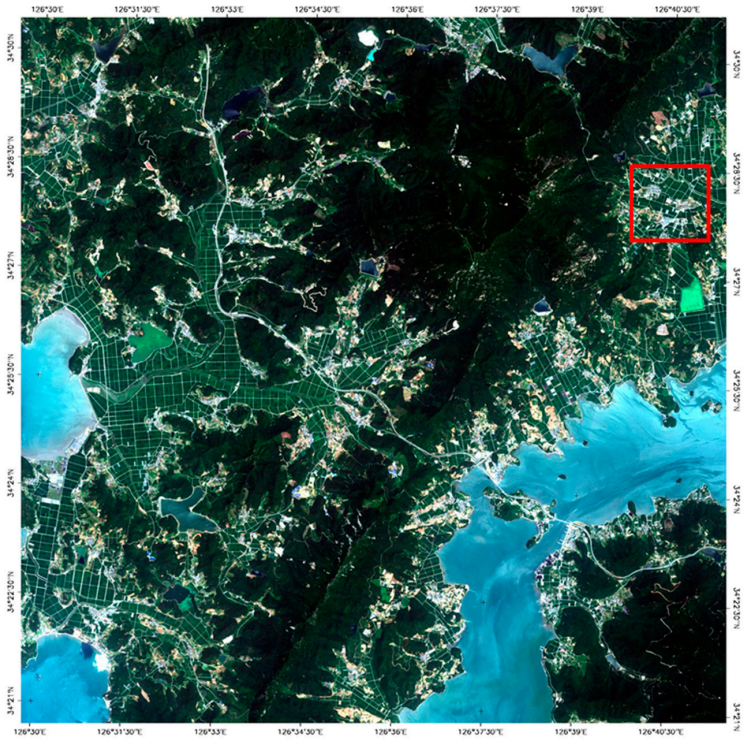

(a)

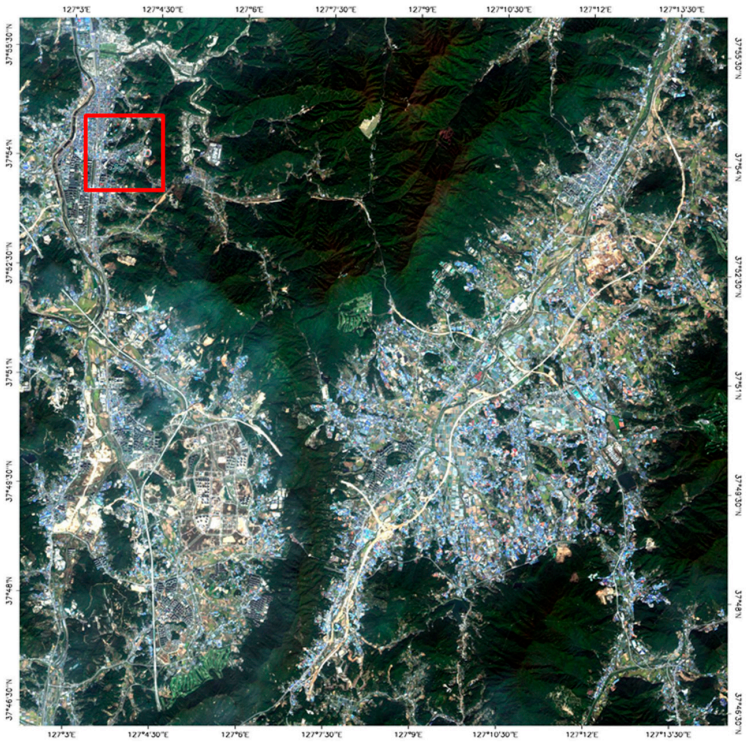

(b)

Figure 1. Study areas for the sharpening of Sentienl-2A imagery: (**a**) true color composite of site 1; and (**b**) true color composite of site 2.

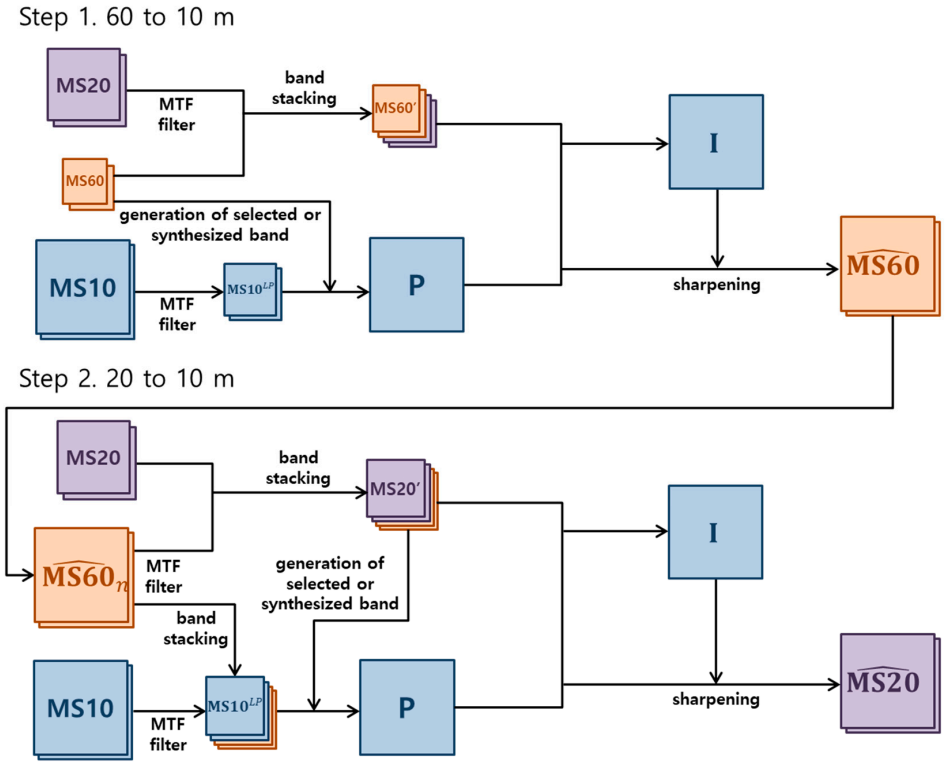

Figure 2. Workflow of the proposed selected and synthesized band scheme.

3.2.1. Sharpening **MS60** with **MS10** and **MS20**

The first step of the proposed band scheme is to sharpen **MS60** from a spatial resolution of 60 m to a spatial resolution of 10 m. In the first step, the key difference between the proposed band scheme and the existing band scheme is that a combination of multispectral images with different spatial resolutions is applied to the multiple linear regression analysis. In each band scheme, $\mathbf{P}_k$ are iteratively selected for every $\mathbf{MS60}_k$ band using correlation analysis (Equations (4) and (5)) or multiple linear regression (Equations (6) and (7)) between $\mathbf{MS10}_n^L$, which has an identical resolution to **MS60**, and $\mathbf{MS60}_k$, depending on whether the selected or synthesized band scheme is used. To generate the optimal $\mathbf{I}_k$, the MTF filter is applied to **MS20** to scale down to the same number of pixels as **MS60**, and the downscaled $\mathbf{MS20}^L$ are stacked with **MS60** with a spatial resolution of 60 m, as shown in Equation (8).

$$\mathbf{MS60}' = \left\{\mathbf{MS20}^L, \mathbf{MS60}\right\} \tag{8}$$

where $\mathbf{MS20}^L$ represents the images that are downscaled to a spatial resolution of 60 m with the MTF filter and $\mathbf{MS60}'$ represents the band-stacked multispectral images with eight bands. MTF can downgrade the spatial resolution of an image [14]. In the first step of the proposed selected band scheme, the stacked $\mathbf{MS60}'$ bands and $\mathbf{P}_k^L$, which is the downscaled image of $\mathbf{P}_k$ to a spatial resolution of 60 m from the MTF filter, are used to produce the $\mathbf{I}_k$. In the MRA-based algorithm, the proposed selected scheme represents an identical pan-sharpening result to the existing selected band scheme because MRA-based algorithms with the proposed and existing selected band schemes generate $\mathbf{I}_k$ using only $\mathbf{P}_k$. However, in CS-based algorithms, the proposed selected and synthesized band schemes are different from the existing band schemes in that $\mathbf{MS60}'$ is used to weighted combinations, such as the average of multispectral images or multiple regression analysis, to generate $\mathbf{I}_k$. For example, the GIHS algorithm generates $\mathbf{I}_k$ using the average of multispectral image, while the GSA algorithm uses multiple regression analysis. In the GSA algorithm, this multiple regression analysis can be defined as shown in Equation (9):

$$\mathbf{P}_k = \omega_{k_0} + \sum_{r=1}^{8} \omega_{k_r} \mathbf{MS60'}_r \tag{9}$$

where ω_{k_r}, which are the weight values that correspond to the rth band of **MS60′**, are determined through the least-squares method, and r is the band number of **MS60′**. Subsequently, $\mathbf{I}_k$ is calculated using Equation (10):

$$\mathbf{I}_k = \omega_{k_0} + \sum_{r=1}^{8} \omega_{k_r} \widetilde{\mathbf{MS60'}}_r \tag{10}$$

Compared to the case where only **MS60** is used in existing band schemes to sharpen Sentinel-2A imagery, a synthetic intensity image that is spectrally similar to $\mathbf{P}_k$ can be generated because the root mean square error (RMSE) of the regression analysis can be greatly reduced when **MS60′** is used. Therefore, the spectral distortion that occurs in the CS-based sharpening algorithm can be greatly reduced through the proposed band schemes. After calculating $\mathbf{P}_k$ and $\mathbf{I}_k$, the sharpened image $\widehat{\mathbf{MS60}}_k$ can be calculated using Equation (11):

$$\widehat{\mathbf{MS60}}_k = \widetilde{\mathbf{MS60}}_k + \mathrm{g}_k(\mathbf{P}_k - \mathbf{I}_k),\ k = 1, 2 \tag{11}$$

3.2.2. Sharpening **MS20** with **MS10** and $\widehat{\mathbf{MS60}}$

In the second step of the proposed band schemes, $\widehat{\mathbf{MS60}}$, which are sharpened to a spatial resolution of 10 m by Equation (11), are used as if they were included in the **MS10** and **MS20** dataset with a spatial resolution of 10 and 20 m, respectively. The new band-stacked multispectral images **MS10′** and **MS20′** are defined using Equations (12) and (13):

$$\mathbf{MS10'} = \left\{ \mathbf{MS10}, \widehat{\mathbf{MS60}} \right\} \tag{12}$$

$$\mathbf{MS20'} = \left\{ \mathbf{MS20}, \widehat{\mathbf{MS60}}^{L} \right\} \tag{13}$$

where $\widehat{\mathbf{MS60}}^{L}$ represents the images that are downscaled by the MTF filter to a spatial resolution of 20 m based on the sharpened image $\widehat{\mathbf{MS60}}$. By adding $\widehat{\mathbf{MS60}}$ from the first step to the set of **MS10**, as shown in Equation (14), we increased the number of **MS10** bands that are likely to have similar spectral characteristics to **MS20** in both the selected and synthesized band schemes. This approach may increase the probability that a band with the most similar characteristics to a specific band of **MS20** is selected. In addition, we attempted to reduce the RMSE of the regression analysis to generate **I** in the CS-based algorithm by adding **MS60** to the band set of **MS20**. Therefore, the sharpened **MS60** was re-applied to the sharpening framework for Sentinel-2A imagery in the second step to improve the spectral quality of optimal panchromatic bands and synthetic intensity images. Using **MS10′** instead of **MS10**, the set of the optimal panchromatic images $\mathbf{P}_m$ was calculated via Equations (4) and (5) or Equations (6) and (7) according to a specific band scheme. Then, $\mathbf{I}_m$ was determined by the image degradation of $\mathbf{P}_m$ or multiple linear regression between $\mathbf{P}_m^L$ and **MS20′**. Finally, the sharpened image could be extracted using Equation (14):

$$\widehat{\mathbf{MS20}}_m = \widetilde{\mathbf{MS20}}_m + g_m(\mathbf{P}_m - \mathbf{I}_m),\ m = 1, \ldots, 6 \tag{14}$$

3.3. Experimental Methods for the Quality Evaluation of Sharpened Images

The general CS- and MRA-based pan-sharpening algorithms were applied to Sentinel-2A imagery using the existing selected and synthesized band scheme to evaluate the performance of our proposed selected and synthesized band scheme. For the existing pan-sharpening algorithms, we selected the GSA and GIHS for the CS-based algorithms and GS2 and MTF-GLP for the MRA-based algorithms. The GSA algorithm, which was proposed by Aiazzi et al. [21], uses an intensity image that is produced from multiple

regression, and its pan-sharpened results are known to be superior to other CS-based fusion results [33]. The GS2 algorithm's method for extracting injection gains is identical to that of the GSA algorithm; however, in the GS2 algorithm, an MTF filter is used to perform image degradation during synthetic intensity image generation. GIHS was developed to improve the spectral distortion problem from IHS [35,36]. IHS-based pan-sharpening algorithms generate a synthetic intensity image through an average of multispectral images. The MTF-GLP is an algorithm that is used in the frequency analysis of panchromatic images, which uses digital filters with frequency responses and includes a model of the MTF of the imaging system [37]. The GIHS and MTF-GLP methods use equivalent injection gains, which are all set to 1.

Quantitative and qualitative evaluations were performed on the pan-sharpened Sentinel-2 images that were generated after applying each algorithm. A qualitative evaluation was performed though visual inspection. Meanwhile, no reference image existed for a comparison with the sharpened image. Consistency measurements are known to be efficient at estimating a sharpened image without a reference image [38]. A sharpened image was generated from the original satellite dataset. Then, the spatial resolution of the sharpened image was degraded to that of the original multispectral image, and the degraded sharpened image was quantitatively compared to the original multispectral image. The erreur relative global adimensionnelle de synthese (ERGAS), spectral angle mapper (SAM) method, universal image quality index (UIQI), and spatial correlation coefficient (sCC) were used to evaluate the spectral-spatial accuracy as the evaluation indices for the quantitative evaluation. The ERGAS is an index for evaluating the global spectral quality between corresponding bands of original and fused images and is defined as shown in Equation (15) [18,39]:

$$\mathrm{ERGAS} = 100\frac{h}{l}\sqrt{\frac{1}{K}\sum_{l=1}^{L}\left(\frac{RMSE^2(i)}{MEAN(i)}\right)} \tag{15}$$

where h is the spatial resolution of the sharpened image, l is the spatial resolution of the multispectral image, K is the number of bands in the sharpened image $\widehat{\mathbf{MS}}$, $MEAN(i)$ is the average value of the lth band, and RMSE is defined according to Equation (16):

$$\mathrm{RMSE} = \frac{1}{MN}\sqrt{\sum_{i,j=1}^{MN}\left(\widehat{\mathbf{MS}}^{L}(i,j) - \mathbf{MS}(i,j)\right)^2} \tag{16}$$

where $M \times N$ is the image size, $\widehat{\mathbf{MS}}^{L}(i,j)$ is the pixel value of the sharpened image, and $\mathbf{MS}(i,j)$ is the pixel value of the original multispectral image. Therefore, $RMSE^2(i)$ indicates the RMSE between the ith band of $\widehat{\mathbf{MS}}$ and $\mathbf{MS}$. Low ERGAS values correspond to small amounts of spectral distortion.

The SAM method calculates the spectral distortion between two vectors and is defined according to Equation (17) [19,40]:

$$\mathrm{SAM}(v,\widehat{v}) = \arccos\left(\frac{\langle v,\widehat{v}\rangle}{\|v\|_2\|\widehat{v}\|_2}\right) \tag{17}$$

where v is the spectral pixel vector of the original multispectral band and $\widehat{v}$ is the pixel vector of the sharpened band. When the value of SAM equals 0, the spectral distortion is minimal.

The UIQI evaluates the similarity between two images. The evaluation items are the correlation, radiometric distortion, and contrast distortion [41–43]. The UIQI is calculated from Equation (18):

$$\mathrm{Q}(x,y) = \frac{4\sigma_{xy}\overline{x}\,\overline{y}}{\left(\sigma_x^2+\sigma_y^2\right)\left(\overline{x}^2+\overline{y}^2\right)} \tag{18}$$

where x and y are the original and sharpened images, respectively; σ_{xy} is the covariance between x and y; and $\overline{x}$ and $\overline{y}$ denote the variance of x and y, respectively. When the UIQI value is close to 1, the lowest spectral distortion is observed.

The sCC is an index for evaluating the spatial detail between two images. The sCC is calculated using two steps [41]. First, spatially detailed information is extracted by applying a Laplacian filter to the two images to be evaluated. Second, the correlation between the two filtered images is calculated. A high sCC value indicates a high degree of consistency among many of the spatial details in the two evaluated images.

4. Experimental Results

The sharpened results of the Sentinel-2A imagery are evaluated and analyzed in this section. The CS- and MRA-based algorithms were applied to the proposed sharpening workflow. The results of the proposed methods were compared to the results of the selected and synthesized band schemes. Tables 2 and 3 show the evaluation indices used in the quantitative evaluation. The quantitative evaluation was performed in spectral-spatial terms by calculating the fusion evaluation index. The quantitative evaluation was calculated using the sharpening results and the resampled original image. We evaluated the sharpening quality according to the 20 and 60 m bands to confirm the feasibility of the proposed method for various bands. Table 2 shows the CS-based sharpening results, and Table 3 lists the MRA-based sharpening results.

Table 2. Quantitative evaluation results of the component substitution (CS)-based sharpening algorithms.

Site 1									
Quality Index	**Spatial Resolution**	**Existing Method**				**Proposed Method**			
		Selected Band		**Synthesized Band**		**Selected Band**		**Synthesized Band**	
		GSA	**GIHS**	**GSA**	**GIHS**	**GSA**	**GIHS**	**GSA**	**GIHS**
ERGAS	20 m	3.5066	3.4953	4.5216	4.3303	**3.1544**	3.1976	4.4168	4.0500
	60 m	1.1654	6.9007	0.9441	0.8968	**0.2423**	1.9583	0.3951	0.3930
SAM	20 m	1.3788	1.4288	1.9899	1.9158	**1.1660**	1.2646	1.7488	1.6979
	60 m	1.1889	6.9251	0.9622	0.9157	**0.2049**	1.7763	0.3867	0.3847
UIQI	20 m	0.9633	0.9615	0.9465	0.9493	**0.9702**	0.9665	0.9505	0.9528
	60 m	0.9377	0.6187	0.9473	0.9514	**0.9891**	0.8536	0.9807	0.9808
sCC	20 m	0.9629	0.9726	0.8350	0.8352	0.9639	**0.9731**	0.8229	0.8232
	60 m	0.9999	0.9735	0.8717	0.8718	**0.9999**	0.9740	0.8717	0.8717
Site 2									
Quality Index	**Spatial Resolution**	**Existing Method**				**Proposed Method**			
		Selected Band		**Synthesized Band**		**Selected Band**		**Synthesized Band**	
		GSA	**GIHS**	**GSA**	**GIHS**	**GSA**	**GIHS**	**GSA**	**GIHS**
ERGAS	20 m	3.6238	3.4461	4.1570	4.0189	3.1343	**3.0797**	3.5829	3.5178
	60 m	0.7215	1.7411	0.7031	0.6500	**0.2903**	0.7687	0.3027	0.3016
SAM	20 m	1.6519	1.5542	1.9422	1.8691	1.5216	**1.4444**	1.8266	1.7893
	60 m	1.0789	2.6063	1.0515	0.9715	**0.3907**	1.0822	0.4483	0.4465
UIQI	20 m	0.9562	0.9580	0.9505	0.9524	**0.9687**	0.9665	0.9648	0.9655
	60 m	0.9717	0.9024	0.9725	0.9753	**0.9902**	0.9607	0.9882	0.9883
sCC	20 m	**0.9801**	0.9733	0.9004	0.9006	0.9777	0.9723	0.9063	0.9070
	60 m	0.9999	0.9968	0.9822	0.9822	**0.9999**	0.9974	0.9822	0.9822

Table 2 shows the results of the quantitative evaluation of the CS-based sharpening results. The sharpened results from the GSA and GIHS method-based selected band scheme show lower ERGAS/SAM values and higher UIQI/sCC values than those from the synthesized band scheme. These results indicate that the selected band scheme is more efficient in the CS-based sharpening of Sentienl-2A imagery than the synthesized band scheme. In addition, the sharpening results of the

proposed selected and synthesized band scheme show better spectral and spatial quality than the existing selected and synthesized band scheme by Wang et al. [7]. At site 1, the GSA sharpening results of the proposed selected band scheme have the highest spectral and spatial qualities of any other algorithm. At site 2, the GSA sharpening results of the proposed selected band scheme show the highest UIQI/sCC values and the lowest ERGAS/SAM values in the 60 m bands. The GIHS sharpening results of the proposed selected band scheme have the lowest ERGAS and SAM values in the 20 m bands. However, the MRA-based sharpening results, which are shown in Table 3, differ from the CS-based sharpening results. The MRA-based sharpening results from the existing selected band scheme have identical spectral and spatial quality indices to those of the proposed selected band scheme. This result was obtained because the selected panchromatic image in the proposed selected band scheme was equivalent to the panchromatic image in the existing selected band scheme when selecting the band with the highest correlation. No additional information was available to generate a panchromatic image with multiple linear regression analysis, so these trends also occurred in the sharpening results of images with a spatial resolution of 60 m when using the synthesized band scheme. However, for ERGAS, SAM, and UIQI, which are spectral evaluation indices, the sharpening results of bands with 20 m spatial resolution showed high spectral qualities when the proposed synthesized band scheme was applied. In particular, the sharpened images of bands with 20 m spatial resolution from an MTF-GLP based on the proposed synthesized band scheme present the best ERGAS, SAM, and UIQI values relative to the sharpening results from other existing methods and the proposed selected band scheme algorithms. In addition, the proposed selected band scheme with the highest sharpening quality in the CS-based algorithm was compared to the proposed synthesized band scheme with the highest sharpening quality in the MRA-based algorithm. The results show that the CS-based method is superior in terms of spatial quality but that the MRA-based method is superior in terms of spectral quality. For visual comparison, Figures 3–6 show detailed images of the sharpened results for the two study areas, which are shown in the red box in Figure 1.

Table 3. Quantitative evaluation results of the multiresolution analysis (MRA)-based sharpening algorithms.

Site 1									
Quality Index	**Spatial Resolution**	**Existing Method**				**Proposed Method**			
		Selected Band		**Synthesized Band**		**Selected Band**		**Synthesized Band**	
		GS2	**MTF-GLP**	**GS2**	**MTF-GLP**	**GS2**	**MTF-GLP**	**GS2**	**MTF-GLP**
ERGAS	20 m	2.8836	2.9283	1.9841	1.9830	2.8836	2.9283	1.9752	**1.9741**
	60 m	0.1480	1.9047	0.1722	0.1722	**0.1480**	1.9047	0.1722	0.1722
SAM	20 m	0.8721	0.9331	0.6950	0.6946	0.8721	0.9331	0.6935	**0.6931**
	60 m	0.1400	1.7074	0.1624	0.1624	**0.1400**	1.7074	0.1624	0.1624
UIQI	20 m	0.9746	0.9736	0.9888	0.9888	0.9746	0.9736	0.9888	**0.9888**
	60 m	0.9963	0.8620	0.9954	0.9954	**0.9963**	0.8620	0.9954	0.9954
sCC	20 m	0.9483	0.9606	0.8310	0.8310	0.9483	**0.9606**	0.8308	0.8308
	60 m	0.9998	0.9741	0.8716	0.7479	**0.9998**	0.9741	0.8716	0.8716
Site 2									
Quality Index	**Spatial Resolution**	**Existing Method**				**Proposed Method**			
		Selected Band		**Synthesized Band**		**Selected Band**		**Synthesized Band**	
		GS2	**MTF-GLP**	**GS2**	**MTF-GLP**	**GS2**	**MTF-GLP**	**GS2**	**MTF-GLP**
ERGAS	20 m	2.9692	2.9660	2.0766	2.0756	2.9692	2.9660	2.0711	**2.0702**
	60 m	0.1975	0.7046	0.2042	0.2042	**0.1975**	0.7046	0.2042	0.2042
SAM	20 m	1.2332	1.2404	1.5023	1.0517	1.2332	1.2404	1.5012	**1.0505**
	60 m	0.2876	1.0236	0.2967	0.2967	**0.2876**	1.0236	0.2967	0.2967
UIQI	20 m	0.9666	0.9664	0.9854	0.9854	0.9666	0.9664	0.9854	**0.9855**
	60 m	0.9958	0.9678	0.9955	0.9955	**0.9958**	0.9678	0.9955	0.9955
sCC	20 m	0.9653	0.9585	0.8938	0.8938	**0.9653**	0.9585	0.8936	0.8936
	60 m	0.9998	0.9974	0.9821	0.9821	**0.9998**	0.9974	0.9821	0.9821

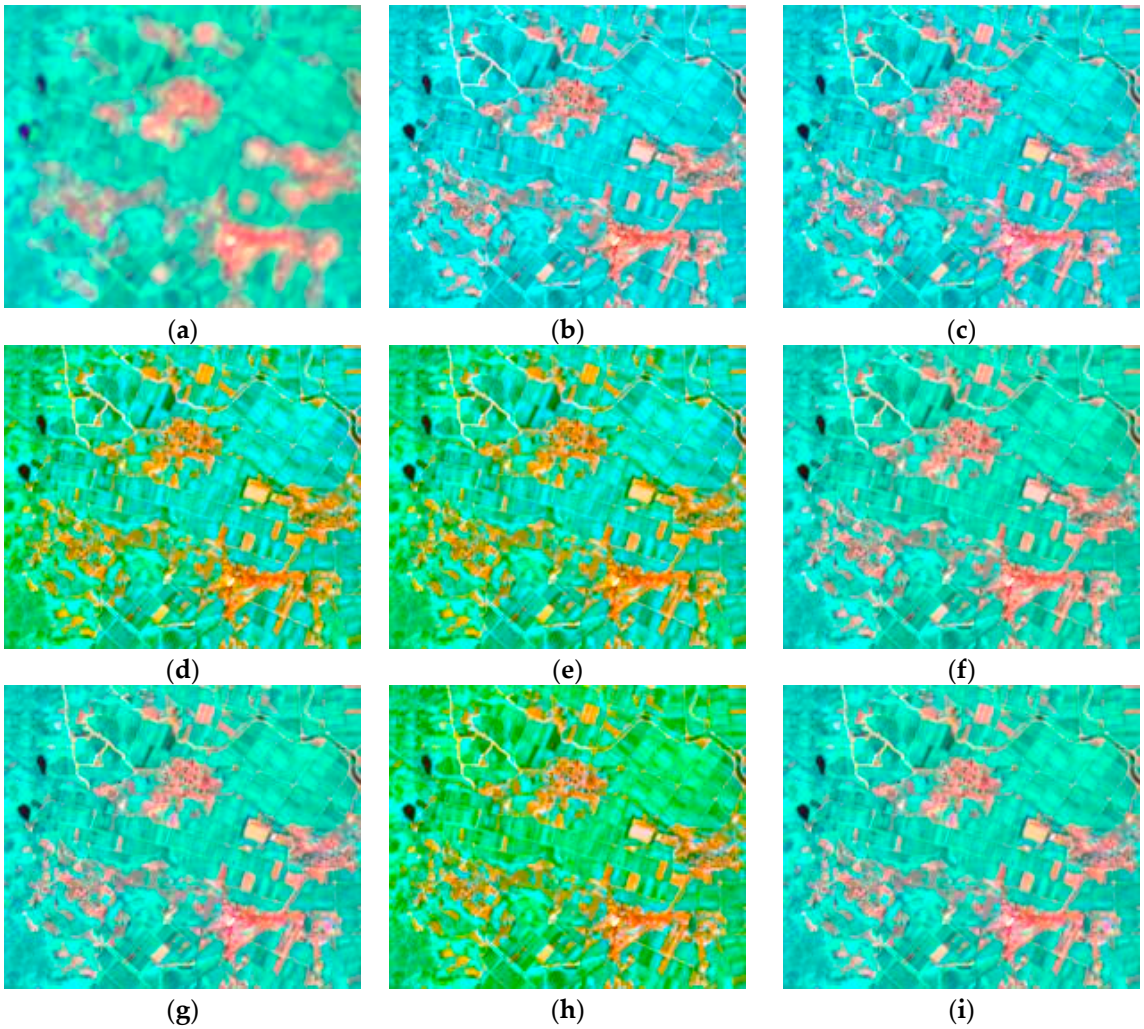

Figure 3. CS-based sharpening results for study area 1 (bands 1, 8a, and 9 are shown as RGB): (**a**) resampled original image; (**b**) GSA result from the existing selected band scheme; (**c**) GSA result from the existing synthesized band scheme; (**d**) GIHS result from the existing selected band scheme, (**e**) GIHS result from the existing synthesized band scheme; (**f**) GSA result from the proposed selected band scheme; (**g**) GSA result from the proposed synthesized band scheme; (**h**) GIHS result from the proposed selected band scheme; and (**i**) GIHS result from the proposed synthesized band scheme.

Figures 3 and 4 show the results of the CS-based sharpening, and Figures 5 and 6 show the results of the MRA-based sharpening for the two study areas. Panels (b−e) in Figures 3–6 show the results when using the existing method, and panels (f–i) show the results when applying the proposed method. CS-based algorithms are known to generate more spectral distortion than MRA-based algorithms, so similar results were obtained in this experiment. In Figures 3 and 4, where a CS-based algorithm was used, the spectral characteristics of (b–e) and (f–i) were different. Compared to the resampled original image (Figure 3a), spectral distortion occurred in (b–e) in Figures 3 and 4 when the existing method was used, and these results tended to be brighter and more distorted than the results from the proposed method. As shown in Figure 3d,e,h, the results from the IHS-based algorithms generated **I** using the average of the multispectral images, thus creating large spectral distortion. However, as shown in Figure 3i, the IHS results from the proposed synthesized band scheme showed relatively low spectral distortion because the optimal combination was found before performing the synthesized band scheme. The GSA and GIHS sharpening results from the proposed synthesized band scheme and the GSA results from the proposed selected band scheme showed the best visual quality. Similar spectral results were obtained in the sharpening results of Figures 5 and 6, for which the MRA-based algorithm was

used, although slight spatial distortions such as blurring were created in (b–e) when applying the existing method. When the existing and proposed selected band schemes were used, the highest spectral distortion occurred when the CS-based GIHS and MRA-based MTF-GLP algorithms, which set g_n equal to 1, were applied. However, many of the spectral distortions were visually reduced when the same algorithms were applied to the proposed synthesized band scheme. The qualitative evaluation showed that the sharpening results from the synthesized band scheme were better than those from the selected band scheme, and the sharpening quality was improved in terms of the spectral-spatial aspects when sharpening was performed with the proposed selected and synthesized methods rather than the existing methods.

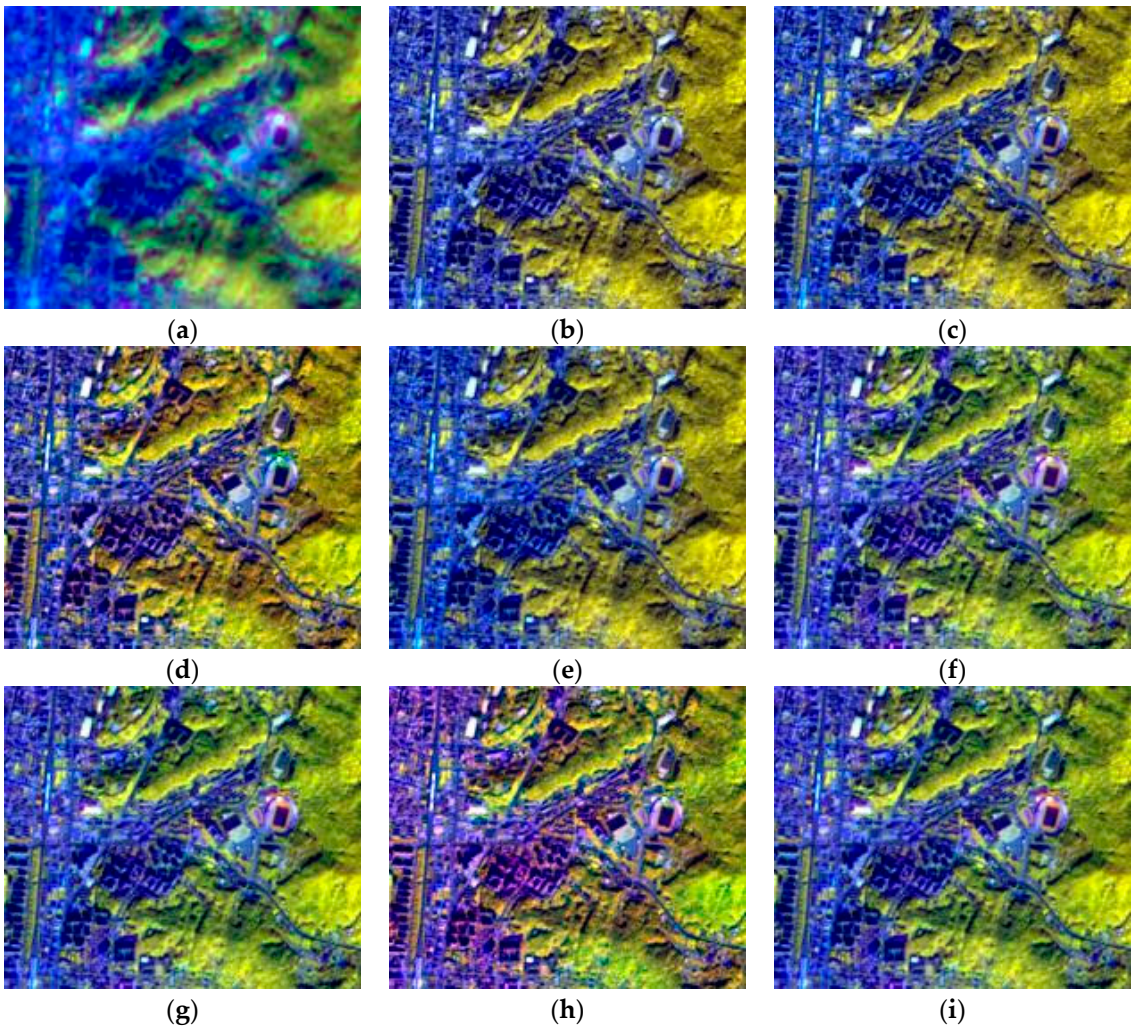

Figure 4. CS-based sharpening results for study area 2 (bands 9, 7, and 1 are shown as RGB): (**a**) resampled original image; (**b**) GSA result from the existing selected band scheme; (**c**) GSA result from the existing synthesized band scheme; (**d**) GIHS result from the existing selected band scheme; (**e**) GIHS result from the existing synthesized band scheme; (**f**) GSA result from the proposed selected band scheme; (**g**) GSA result from the proposed synthesized band scheme; (**h**) GIHS result from the proposed selected band scheme; and (**i**) GIHS result from the proposed synthesized band scheme.

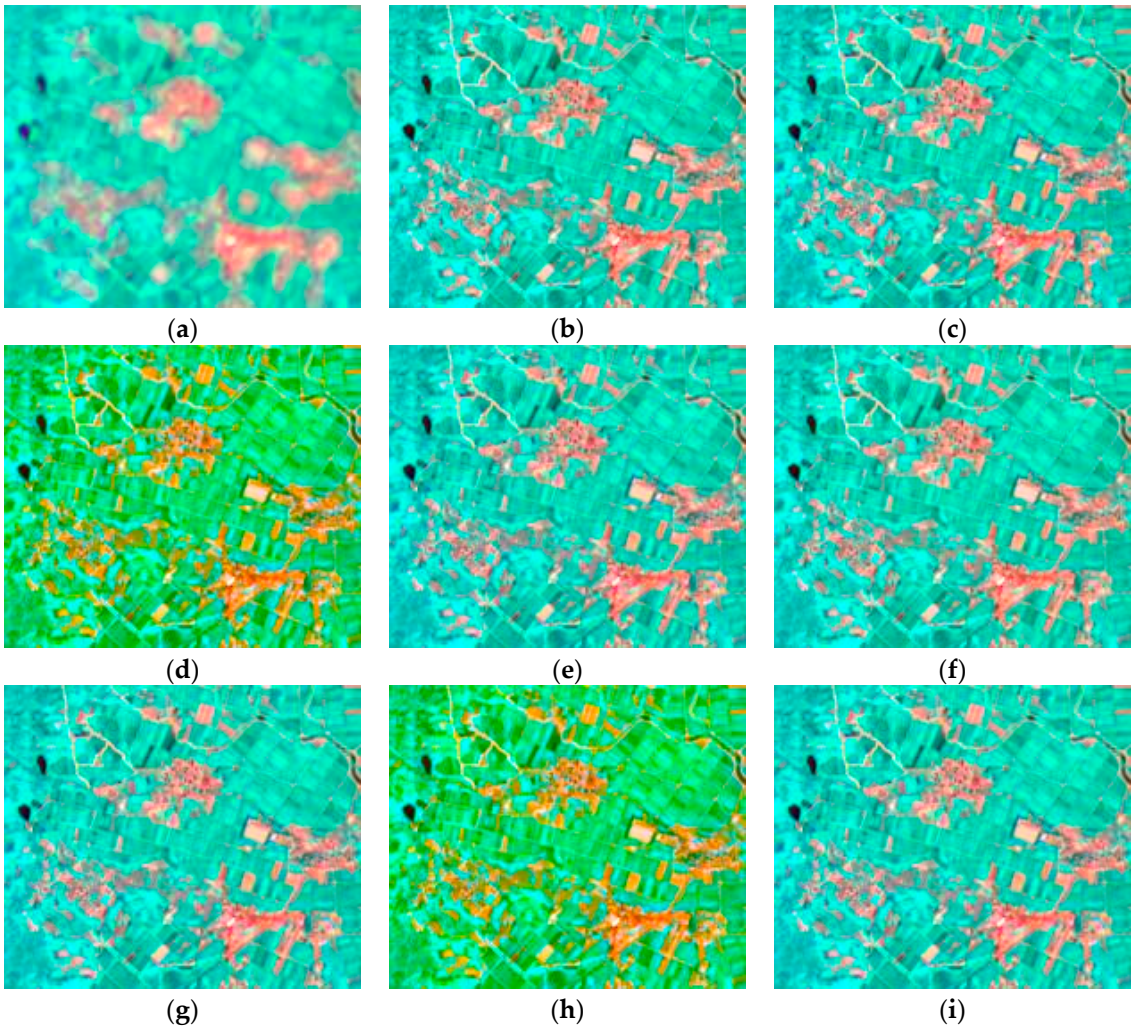

Figure 5. MRA-based sharpening results for study area 1 (bands 1, 8a, and 9 are shown as RGB): (**a**) resampled original image; (**b**) GS2 result from the existing selected band scheme; (**c**) GS2 result from the existing synthesized band scheme; (**d**) MTF-GLP result from the existing selected band scheme; (**e**) MTF-GLP result from the existing synthesized band scheme; (**f**) GS2 result from the proposed selected band scheme; (**g**) GS2 result from the proposed synthesized band scheme; (**h**) MTF-GLP result from the proposed selected band scheme; and (**i**) MTF-GLP result from the proposed synthesized band scheme.

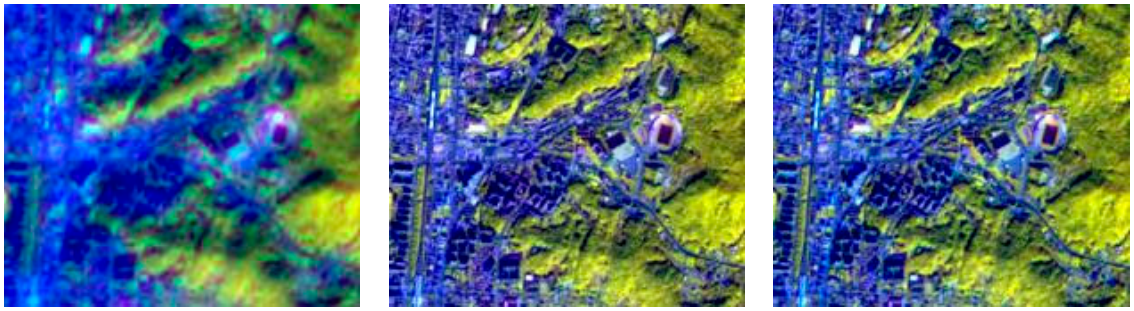

Figure 6. *Cont.*

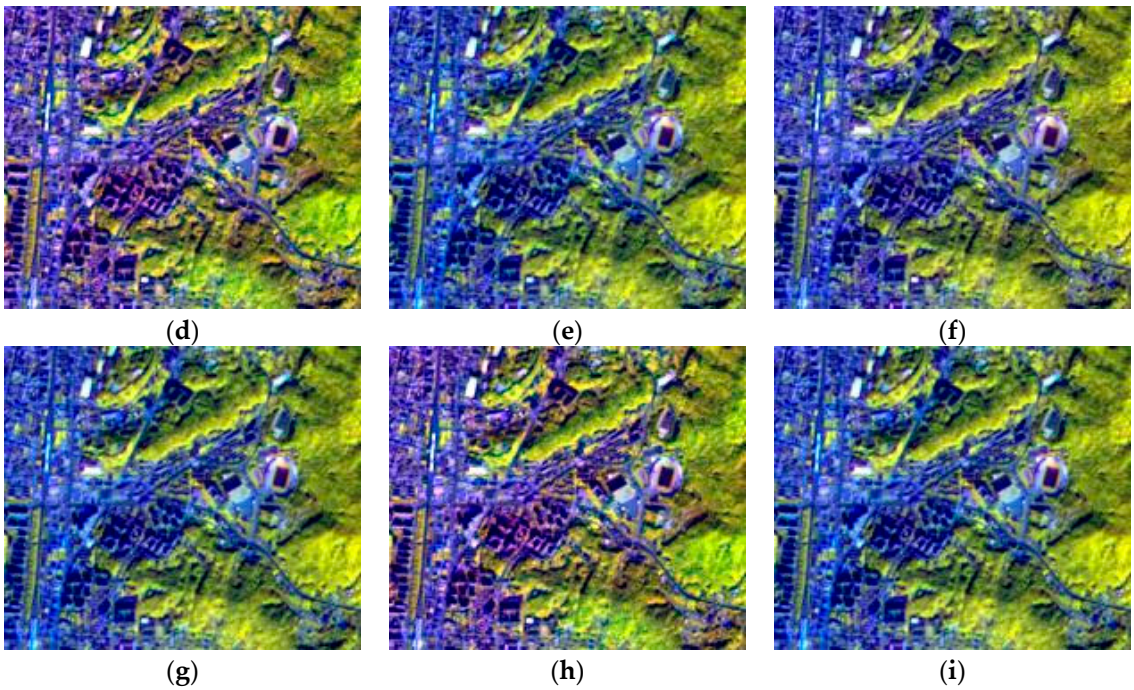

Figure 6. MRA-based sharpening results for study area 2 (bands 9, 7, and 1 are shown as RGB): (**a**) resampled original image; (**b**) GS2 result from the existing selected band scheme; (**c**) GS2 result from the existing synthesized band scheme; (**d**) MTF-GLP result from the existing selected band scheme; (**e**) MTF-GLP result from the existing synthesized band scheme; (**f**) GS2 result from the proposed selected band scheme; (**g**) GS2 result from the proposed synthesized band scheme; (**h**) MTF-GLP result from the proposed selected band scheme; and (**i**) MTF-GLP result from the proposed synthesized band scheme.

5. Discussion

In this manuscript, we proposed sharpening methods for Sentinel-2A imagery based on selected and synthesized band schemes. Evaluations of the proposed method in two studies yielded the following findings:

(1) The sharpening result from GSA based on the proposed selected band scheme quantitatively and qualitatively demonstrated the best quality when compared to the other results from the CS-based algorithms. As shown in Figure 7, the sharpening results from the proposed selected band scheme had lower ERGAS/SAM and higher UIQI/sCC values than those from the proposed synthesized band scheme. The sharpening of **MS20** and **MS60** produced similar tendencies. In addition, the quality improvement of the results from the proposed selected band scheme was further enhanced compared to the results from the synthesized band scheme. This observation suggests that the **P**, generated by the selected band scheme, while generating **I** with a weighted combination of multispectral images, more strongly minimized the spectral distortion.

(2) The existing and proposed algorithms based on the selected band scheme showed the same quality when sharpening the 60 m spatial resolution bands because the selected bands were identical to each other when selecting the band with the highest correlation. However, when applied to 20 m spatial resolution bands, the spectral quality was slightly higher than that of the proposed synthesized band scheme. As shown in Figure 8, the sharpening results from the MTF-GLP based on the proposed synthesized band scheme produced the best spectral quality when sharpening 20 m spatial resolution bands. The optimal **I** was only generated from the set of optimal panchromatic bands **P** in the MRA-based algorithm, so the **P** from the synthesized band scheme was the more critical parameter for spectral enhancement in the sharpening of Sentinel-2A imagery.

(3) The spatial characteristics of the sharpening results were significantly different when applying the CS-based algorithms to the proposed selected and synthesized band schemes. Figure 9 shows a zoomed image of the result when applying the CS-based GSA algorithm to the proposed methods. The zoomed images show that the selected band scheme emphasized more spatial characteristics than the synthesized band scheme when applying the CS-based algorithm to the proposed method. In terms of spatial detail, the edges of urban objects, such as roads and buildings, were sharpened, and the cropland boundaries could be identified.

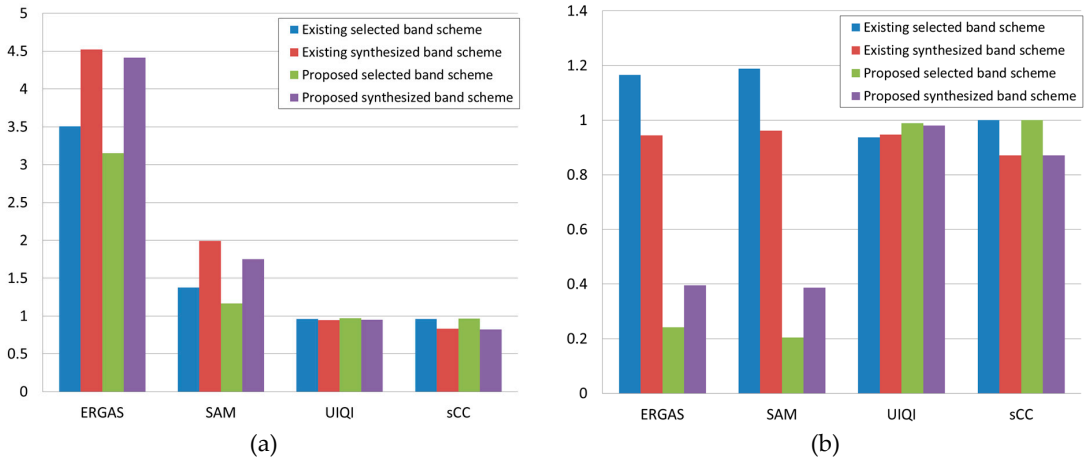

Figure 7. Sharpening results from the existing and proposed methods when applying the GSA algorithm to study area 1: (**a**) sharpening results of the 20 m bands; and (**b**) sharpening results of the 60 m bands.

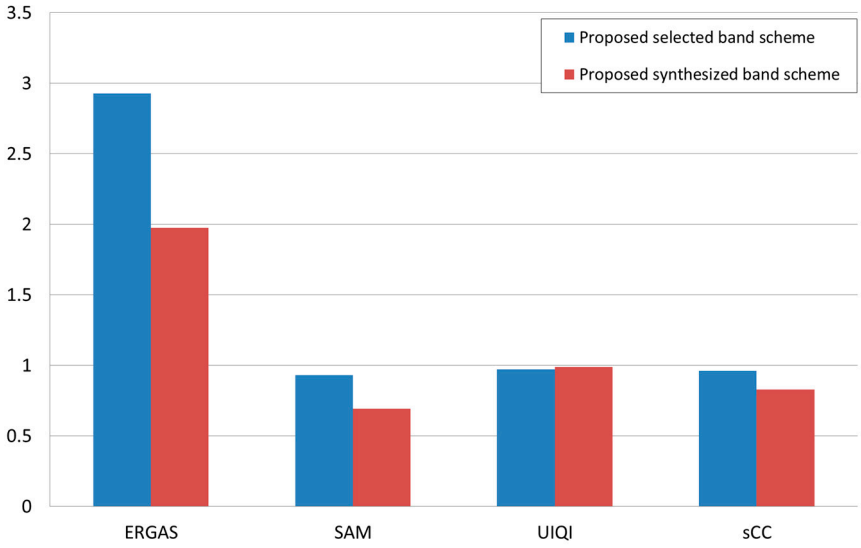

Figure 8. Sharpening results from the proposed selected and synthesized band scheme when applying the MTF-GLP algorithm to study area 1.

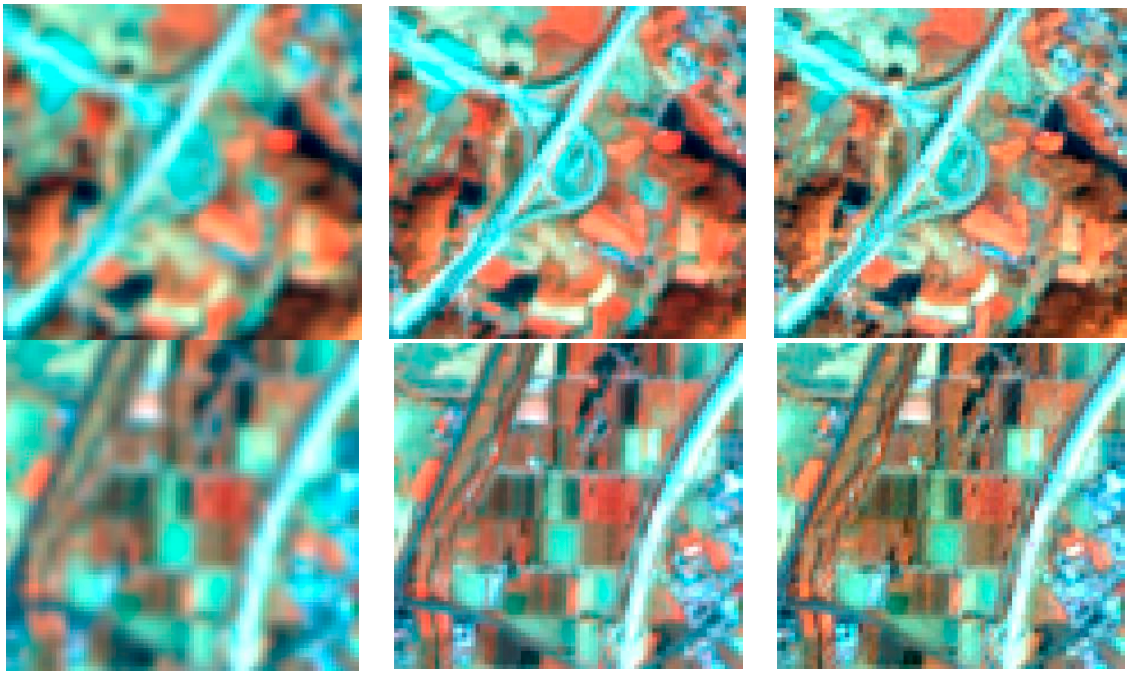

Figure 9. Zoomed images of the sharpening results from the proposed methods when applying the GSA algorithm to study area 2 (bands 8a, 11, and 12 are shown as RGB; upper line is subarea 1 and lower line is subarea 2): (**a**) original spatial resolution image; (**b**) sharpening result from the proposed selected band scheme; (**c**) sharpening result from the proposed synthesized band scheme.

6. Conclusions

The sharpening method proposed in this work represents an improvement over the existing selected and synthesized band schemes. The major difference between the selected and synthesized band methods proposed in this manuscript was observed in the generation of a set of optimal panchromatic images by integrating the original multispectral bands with 20 and 60 m spatial resolution. The experimental results showed that the sharpening results of the proposed sharpening framework were improved in terms of the spatial and spectral properties when compared to the existing selected and synthesized band scheme. However, the results of the sharpening algorithm when applied to the proposed schemes showed different tendencies. In the case of the proposed selected band scheme, the sharpening results by the CS-based algorithms represent higher spatial quality compared to those by the MRA-based algorithms. Conversely, the sharpening results by the MRA-based algorithms showed improved spectral quality when using the proposed synthesized band scheme. Therefore, the sharpened image of Sentinel-2A imagery using the proposed synthesized method with MRA-based algorithms is advantageous for applications based on spectral features, such as image classification and change detection. If spatial clarity is required in the application of remotely sensed imagery, such as in image interpretation and feature extraction, researchers should use the proposed selected method based on CS-based algorithms to sharpen Sentinel-2A imagery. Future research will be conducted to develop optimal sharpening methods for application with other types of satellite images and heterogeneous sensors.

Acknowledgments: This research was supported by Basic Science Research Program through the National Research Foundation of Korea (NRF), which is funded by the Ministry of Education (NRF-2017R1D1A3B03034602).

Author Contributions: Honglyun Park and Jaewan Choi designed the proposed algorithm, implemented the experiments, and wrote the manuscript. Nyunghee Park supported the experiments. Seokkeun Choi provided feedback on the proposed algorithm and reviewed the manuscript.

Conflicts of Interest: The authors declare no conflicts of interest.

References

1. Drusch, M.; Del Bello, U.; Carlier, S.; Colin, O.; Fernandez, V.; Gascon, F.; Hoersch, B.; Isola, C.; Laberinti, P.; Martimort, P.; et al. Sentinel-2: ESA's optical high-resolution mission for GMES operational Services. *Remote Sens. Environ.* **2012**, *120*, 25–36. [CrossRef]
2. Richter, K.; Hank, T.B.; Vuolo, F.; Mauser, W.; D'Urso, G. Optimal exploitation of the Sentinel-2 spectral capabilities for crop leaf area index mapping. *Remote Sens.* **2012**, *4*, 561–582. [CrossRef]
3. Clevers, J.G.P.W.; Gitelson, A.A. Remote estimation of crop and grass chlorophyll and nitrogen content using red-edge bands on Sentinel-2 and 3. *Int. J. Appl. Earth Obs. Geoinf.* **2013**, *23*, 344–351. [CrossRef]
4. Dotzler, S.; Hill, J.; Buddenbaum, H.; Stoffels, J. The potential of EnMAP and Sentinel-2 data for detecting drought stress phenomena in deciduous forest communities. *Remote Sens.* **2015**, *7*, 14227–14258. [CrossRef]
5. Zhang, Y. Understanding image fusion. *Photogramm. Eng. Remote Sens.* **2004**, *70*, 657–661.
6. Alparone, L.; Wald, L.; Chanussot, J.; Thomas, C.; Gamba, P.; Bruce, L.M. Comparison of pansharpening algorithm: Outcome of the 2006 GRS-S Data-Fusion contest. *IEEE Trans. Geosci. Remote Sens.* **2007**, *45*, 3012–3021. [CrossRef]
7. Wang, Q.; Shi, W.; Li, Z.; Atkinson, P.M. Fusion of Sentinel-2 image. *Remote Sens. Environ.* **2016**, *187*, 241–252. [CrossRef]
8. Licciardi, G.A.; Khan, M.M.; Chanussot, J.; Montanvert, A.; Condat, L.; Jutten, C. Fusion of hyperspectral and panchromatic images using multiresolution analysis and nonlinear PCA band reduction. *J. Adv. Signal Process.* **2012**, *1*, 207–223. [CrossRef]
9. Rahmani, S.; Strait, M.; Merkurjev, D.; Moeller, M.; Wittman, T. An adaptive IHS pan-sharpening method. *IEEE Geosci. Remote Sens. Lett.* **2010**, *7*, 746–750. [CrossRef]
10. Aiazzi, B.; Baronti, S.; Selva, M. Improving component substitution pansharpening through multivariate regression of MS+pan data. *IEEE Trans. Geosci. Remote Sens.* **2007**, *45*, 3230–3239. [CrossRef]
11. Shah, V.P.; Younan, N.H.; King, R.L. An efficient pan-sharpening method via a combined adaptive PCA approach and contourlet. *IEEE Trans. Geosci. Remote Sens.* **2008**, *46*, 1323–1335. [CrossRef]
12. Choi, J.; Yu, K.; Kim, Y. A new adaptive component-substitution-based satellite image fusion by using partial replacement. *IEEE Trans. Geosci. Remote Sens.* **2011**, *49*, 295–309. [CrossRef]
13. Kang, X.; Li, S.; Benediktsson, J.A. Pansharpening with matting model. *IEEE Trans. Geosci. Remote Sens.* **2014**, *52*, 5088–5099. [CrossRef]
14. Vivone, G.; Alparone, L.; Chanussot, J.; Mura, M.D.; Garzelli, A.; Licciardi, G.A.; Restaino, R.; Wald, L. A critical comparison among pansharpening algorithm. *IEEE Trans. Geosci. Remote Sens.* **2015**, *53*, 2565–2586. [CrossRef]
15. Pradhan, P.S.; King, R.L.; Younan, N.H.; Holcomb, D.W. Estimation of the number of decomposition levels for a wavelet-based multiresolution multisensory image fusion. *IEEE Trans. Geosci. Remote Sens.* **2006**, *44*, 3674–3686. [CrossRef]
16. Nunez, J.; Otazu, X.; Fors, O.; Prades, A.; Pala, V.; Arbiol, R. Multiresolution-based image fusion with additive wavelet decomposition. *IEEE Trans. Geosci. Remote Sens.* **1999**, *37*, 1204–1211. [CrossRef]
17. Yocky, D.A. Multiresolution wavelet decomposition image merger of Landsat thematic mapper and SPOT panchromatic data. *Photogramm. Eng. Remote Sens.* **1996**, *62*, 1067–1074.
18. Li, S. A new pan-sharpening method using a compressed sensing technique. *IEEE Trans. Geosci. Remote Sens.* **2011**, *49*, 738–746. [CrossRef]
19. Cheng, J.; Liu, H.; Liu, T.; Wang, F.; Li, H. Remote sensing image fusion via wavelet transform and sparse representation. *ISPRS J. Photogramm. Remote Sens.* **2015**, *104*, 158–173. [CrossRef]
20. Garzelli, A.; Nencini, F. Interband structure modeling for pan-sharpening of very high-resolution multispectral images. *Inf. Fusion* **2005**, *6*, 213–224. [CrossRef]
21. Aiazzi, B.; Baronti, S.; Lotti, F.; Selva, M. A comparison between global and context-adaptive pansharpening of multispectral images. *IEEE Geosci. Remote Sens. Lett.* **2009**, *6*, 302–306. [CrossRef]
22. Vaiopoulos, A.D.; Karantzalos, K. Pansharpening on the narrow VNIR and SWIR spectral bands of Sentinel-2. *Int. Arch. Photogramm. Remote Sens. Spat. Inf. Sci.* **2016**, *XLI-B7*, 723–730. [CrossRef]

23. Selva, M.; Aiazzi, B.; Butera, F.; Chiarantini, L.; Baronti, S. Hyper-sharpening: A first approach on SIM-GA data. *IEEE J. Sel. Top. Appl. Earth Obs. Remote Sens.* **2015**, *8*, 3008–3024. [CrossRef]
24. Du, T.; Zhang, Y.; Ling, F.; Wang, Q.; Li, W.; Li, X. Water bodies' mapping from Sentinel-2 imagery with modified normalized difference water index at 10 m spatial resolution produced by sharpening the SWIR band. *Remote Sens.* **2016**, *8*, 354. [CrossRef]
25. European Space Agency (ESA). *GMES Sentinel-2 Mission Requirements Document*; ESA: Paris, France, 2007.
26. Verrelst, J.; Munoz, J.; Alonso, L.; Delegido, J.; Rivera, J.P.; Camps-Valls, G.; Moreno, J. Machine learning regression algorithms for biophysical parameter retrieval: Opportunities for Sentinel-2 and -3. *Remote Sens. Environ.* **2012**, *118*, 127–139. [CrossRef]
27. Hagolle, O.; Huc, M.; Pascual, D.V.; Dedieu, G. A multi-temporal method for cloud detection, applied to Formosat-2, Venus, Landsat and Sentinel-2 images. *Remote Sens. Environ.* **2010**, *114*, 1747–1755. [CrossRef]
28. Garzelli, A. Pansharpening of multispectral images based on nonlocal parameter optimization. *IEEE Trans. Geosci. Remote Sens.* **2015**, *53*, 2096–2107. [CrossRef]
29. Hallabia, H. High spectral quality pansharpening approach based on MTF-matched filter banks. *Multidimens. Syst. Signal Process.* **2016**, *27*, 831–861. [CrossRef]
30. Wang, Q.; Shi, W.; Atkinson, P.M. Area-to-point regression kriging for pan-sharpening. *ISPRS J. Photogramm. Remote Sens.* **2016**, *114*, 151–165. [CrossRef]
31. El-Mezouar, M.C.; Kpalma, K.; Taleb, N.; Ronsin, J. A pan-sharpening based on the non-subsampled contourlet transform: Application to Worldview-2 imagery. *IEEE J. Sel. Top. Appl. Earth Obs. Remote Sens.* **2014**, *7*, 1806–1815. [CrossRef]
32. Li, H.; Jing, L.; Tang, Y. Assessment of pansharpening method applied to Worldview-2 imagery fusion. *Sensors* **2017**, *17*, 89. [CrossRef] [PubMed]
33. Choi, J.; Yeom, J.; Chang, A.; Byun, Y.; Kim, Y. Hybrid pansharpening algorithm for high spatial resolution satellite imagery to improve spatial quality. *IEEE Geosci. Remote Sens. Lett.* **2013**, *10*, 490–494. [CrossRef]
34. European Space Agency (ESA). *Sentinel-2 Data Quality Report*; ESA: Paris, France, 2017.
35. Oh, K.Y.; Jung, H.S.; Jeong, N.K.; Lee, K.J. The comparative analysis of image fusion results by using KOMPSAT-2/3 images. *J. Korean Soc. Surv. Geodesy Photogramm. Cartogr.* **2014**, *32*, 117–132. [CrossRef]
36. Tu, T.; Huang, P.S.; Hung, C.; Chang, C. A fast intensity-hue-saturation fusion technique with spectral adjustment for IKONOS imagery. *IEEE Geosci. Remote Sens. Lett.* **2004**, *1*, 309–312. [CrossRef]
37. Aiazzi, B.; Alparone, L.; Baronti, S.; Garzelli, A.; Selva, M. MTF-tailored multiscale fusion of high-resolution MS and PAN imagery. *Photogramm. Eng. Remote Sens.* **2006**, *5*, 591–596. [CrossRef]
38. Palsson, F.; Sveinsson, J.R.; Ulfarsson, M.O.; Benediktsson, J.A. Quantitative quality evaluation of pansharpened imagey: Consistency versus synthesis. *IEEE Trans. Geosci. Remote Sens.* **2015**, *54*, 1247–1259. [CrossRef]
39. Guo, Q.; Chen, S.; Leung, H.; Liu, S. Covariance intersection based image fusion technique with application to pansharpening in remote sensing. *Inf. Sci.* **2010**, *180*, 3434–3443. [CrossRef]
40. Wei, Q.; Bioucas-Dias, J.; Dobigeon, N.; Tourneret, J.Y. Hyperspectral and multispectral image fusion based on a sparse representation. *IEEE Trans. Geosci. Remote Sens.* **2015**, *53*, 3658–3668. [CrossRef]
41. Mahyari, A.G.; Yazdi, M. Panchromatic and multispectral image fusion based on maximization of both spectral and spatial similarities. *IEEE Trans. Geosci. Remote Sens.* **2011**, *49*, 1976–1985. [CrossRef]
42. Alparone, L.; Aiazzi, B.; Baronti, S.; Garzelli, A.; Nencini, F.; Selva, M. Multispectral and panchromatic data fusion assessment without reference. *Photogramm. Eng. Remote Sens.* **2008**, *74*, 193–200. [CrossRef]
43. Wang, Z.; Bovik, A.C. A universal image quality index. *IEEE Geosci. Remote Sens. Lett.* **2002**, *9*, 81–84.